Frontiers of Information Technology & Electronic Engineering
www.jzus.zju.edu.cn; engineering.cae.cn; www.springerlink.com
ISSN 2095-9184 (print); ISSN 2095-9230 (online)
E-mail: jzus@zju.edu.cn

Correspondence:

Compact millimeter-wave air-filled substrate-integrated waveguide crossover employing homogeneous cylindrical lens*#

Chun GENG[1,3], Jiwei LIAN[†‡2,3], Dazhi DING[2]

[1]*Qian Xuesen College, Nanjing University of Science and Technology, Nanjing 210094, China*

[2]*School of Microelectronics (School of Integrated Circuits), Nanjing University of Science and Technology, Nanjing 210094, China*

[3]*State Key Laboratory of Millimeter Waves, Southeast University, Nanjing 210096, China*

[†]Email: lianjiwei@njust.edu.cn

Received Oct. 12, 2022; Revision accepted Apr. 18, 2023; Crosschecked Aug. 21, 2023

https://doi.org/10.1631/FITEE.2200454

We propose a new method to design crossovers by employing an embedded homogeneous cylindrical lens (HCL). Compared with traditional crossover designs, this strategy introduces an HCL within the air-filled substrate-integrated waveguide (SIW) crossover cavity to direct the incident waves in the desired direction. According to ray-tracing analysis, the added HCL can efficiently concentrate the electromagnetic wave propagating from the input to the output without increasing the fabrication complexity or footprint. The operating mechanism of this method is elaborated in detail, and is further verified by E-field distributions. Using the air-filled SIW technology, two-, three-, and four-channel crossovers operating at the millimeter-wave are developed and fabricated to demonstrate the practical feasibility of the proposed method. Some transitional structures are designed for experimental purposes. It is found that the simulated fractional bandwidths (FBWs) related to two-, three-, and four-channel air-filled SIW crossovers are 33%, 14%, and 10%, respectively; the dimensions of their core areas are $0.74\lambda\times0.74\lambda$, $1.43\lambda\times1.43\lambda$, and $1.90\lambda\times1.90\lambda$, respectively. Comparisons between our method and similar approaches in the literature illustrate the advantages of our method.

1 Introduction

Couplers are passive components for phase and amplitude allocations between multiple paths (Xu et al., 2011; Niu et al., 2021). Crossovers are referred to as a 0-dB coupler, which enables multiple transmission lines or signal channels to geometrically intersect with each other while maintaining satisfactory isolation among these paths. With the development of microwave and millimeter-wave radio frequency circuits and integrated circuits towards greater compactness and versatility, crossovers inevitably play an increasingly important role as they can effectively address multiple intersection issues (Yao et al., 2011). Taking the Butler matrix (which is a popular feeding network in multibeam antenna designs) as an example, crossovers are required to

‡ Corresponding author

* Project supported by the National Natural Science Foundation of China (Nos. 62101259, 62025109, and 61931021), the National Key Laboratory on Electromagnetic Environment Effects, China (No. JCKYS2019 DC4), the Primary Research and Development Plan of Jiangsu Province, China (No. BE2022070), the Open Research Program of the State Key Laboratory of Millimeter Waves, China (No. K202229), and the Undergraduate Research Training Program of Nanjing University of Science and Technology, China (No. 202210288057)

Electronic supplementary materials: the online version of this article (https://doi.org/10.1631/FITEE.2200454) contains supplementary materials, which are available to authorized users

ORCID: Chun GENG, https://orcid.org/0009-0001-7914-1476; Jiwei LIAN, https://orcid.org/0000-0002-0497-8765

© Zhejiang University Press 2023

connect the couplers and phase shifters, so as to achieve the desired phase gradient (Lian et al., 2018, 2019).

Most reported crossovers operating at the microwave frequency are based on microstrip technology because of its merits of planar structure and ease of integration (Feng et al., 2016; Jiao et al., 2018; Tajik et al., 2018; Yu and Sun, 2019). Recently, millimeter-wave and terahertz applications have attracted great interest due to the higher availability of unallocated frequency spectrum resources. In this situation, some close or quasi-close structures are preferable in crossover designs, which include waveguide (Cheng et al., 2021), substrate-integrated waveguide (SIW) (Djerafi and Wu, 2009; Hesari and Bornemann, 2017; Sun et al., 2020; Qi et al., 2021), and printed ridge gap waveguide (Ali and Sebak, 2018).

Traditional crossovers usually comprise four ports and deal with the intersections between two channels. As the circuit complexity increases, intersections among more than two channels appear and they should be taken into account in circuit designs. One feasible alternative is to cascade multiple two-channel crossovers. For instance, three two-channel crossovers can be combined into a three-channel crossover, or six two-channel crossovers can cooperatively build a four-channel crossover. However, apparently too many two-channel crossovers are required and cascaded in these cases, which can lead to larger sizes and increased losses (Li and Luk, 2016).

Facing this issue, the design of crossovers dealing with more than two channels simultaneously has become a significant and challenging research topic. Tang and Chuang (2015) used double rings in the microstrip to construct a three-channel crossover, which was later extended to a four-channel crossover (Chu and Tang, 2018). Wu et al. (2014) proposed a different three-channel crossover by using lumped inductors. Subsequently, a microstrip three-channel crossover with the filtering property was developed (Wu and Mao, 2016). However, for reasons explained above, these crossovers in the microstrip technology are not suitable for millimeter-wave or above millimeter-wave applications.

Some crossovers have been proposed that use close or quasi-close transmission lines. Using a cavity for excitation TE_{011}, TE_{101}, and TM_{110} modes (Lin et al., 2019), a three-channel waveguide filtering crossover was reported at the expense of a large size. Lian et al. (2020) designed a four-channel crossover using SIW technology by adding a power divider to each port, which eventually led to a larger footprint. When resorting to TE_{102} and TE_{201} modes, four-, five-, and six-channel SIW filtering crossovers have been realized. To support the TE_{102} and TE_{201} modes simultaneously, the whole design is formed by cascaded rectangular cavities, while it suffers from a relatively large footprint (Zhan et al., 2020; Zhou and Wu, 2020).

Given the state-of-the-art development of crossovers, a new method to design air-filled SIW crossovers using an embedded homogeneous cylindrical lens (HCL) was proposed by Geng et al. (2022). In previous studies, HCLs (two-dimensional case) or homogeneous spherical lenses (three-dimensional case) have been widely applied and explored in antenna designs (Bekefi and Farnell, 1956; Gunderson, 1972; Schoenlinner et al., 2002; Boriskin et al., 2008; Costa et al., 2009; Zhang et al., 2011). As for the antenna design, the introduced HCL enables the conversion from spherical or cylindrical wave to planar wave, so that a high-directivity radiation can be achieved. Meanwhile, the feasibility of such lens in crossover designs is still questionable. In the proposed crossover design, the introduced HCL helps concentrate the electromagnetic wave and suppress the wave scattering within the air-filled SIW crossover cavity. Compared with previously published designs, the proposed method has mainly three salient merits. Firstly, this method drills an air-filled area to build an HCL without increasing the crossover footprint. Secondly, it is applicable to the two-channel crossover and can be extended to three-, four-channel crossovers, etc. Thirdly, it can be applied in single-layer SIW technology, which serves as an attractive candidate for low-loss and highly-integrated millimeter-wave applications.

2 Air-filled SIW crossover design

2.1 Operation principle

Fig. 1 depicts the topology of the proposed method for two-, three-, and four-channel crossovers. For the simplest case, it is composed of four ports (two channels). Different from traditional crossover designs, an extra HCL is inserted at the intersection. As a result, the electromagnetic wave coming from port 1 as an

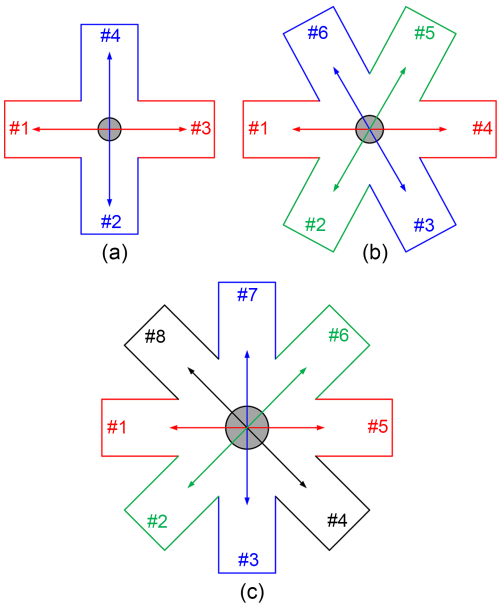

Fig. 1 Topologies of two-channel (a), three-channel (b), and four-channel (c) crossovers

Fig. 1a is reprinted from Geng et al. (2022), Copyright 2022, with permission from IEEE

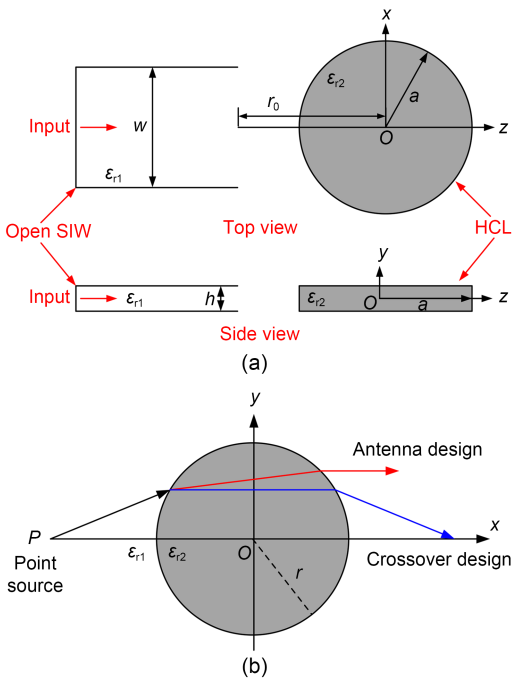

Fig. 2 Design parameters of the HCL (a) and ray-tracing analysis of the crossover with HCL (b)

Fig. 2a is reprinted from Geng et al. (2022), Copyright 2022, with permission from IEEE

example will exclusively propagate toward port 3, while satisfactory isolation is observed between port 1 and port 2 (port 4). This two-channel topology can be extended to three- and four-channel cases by adjusting the diameters of the crossover cavity and the inserted HCL.

Fig. 2a describes the design parameters from both the top view and side view. The width of the open air-filled SIW is denoted by w and the thickness of the substrate is h; a is the radius of the HCL, while r_0 is the distance between the input air-filled SIW and the center of the HCL. The relative dielectric constants inside and outside the HCL are indicated by ε_{r2} and ε_{r1}, respectively.

To further reveal the operation mechanism of the proposed method, the ray-tracing analysis of the crossover with HCL is displayed in Fig. 2b. Lian et al. (2020) demonstrated that concentrating the incoming electromagnetic wave is an effective method to design crossovers, which introduces a power divider at each port, so that the electromagnetic wave is concentrated. At the same time, the added power dividers lead to a larger footprint. In contrast, the proposed topology with an embedded HCL has the merit of better compactness, which is an alternative to concentrating the electromagnetic wave. In this case, the ray escaping out of the HCL should be parallel to the x-axis, as shown in Fig. 2b. In contrast, when designing a crossover, each ray encountering two refractions is expected to arrive at the position mirrored to the source point, as shown in Fig. 2b.

The above is a brief description of the operation mechanism of the proposed method, and a more detailed description can be found in Section 1 of the supplementary materials. More details about this result can be found in (Gunderson, 1972).

To give a clearer view of the impact brought by the HCL, we compute the model using the High-Frequency Structure Simulator (HFSS) and show the E-field distribution, and the results contains two open air-filled SIWs with or without an HCL. As depicted in Figs. 3a and 3b, it is observed that the E-field is bound in the HCL and most of the incoming energy propagates toward the other port. In contrast, if the HCL was removed, the energy would scatter outward and severe energy leakage would appear.

2.2 Design process

Derived from the abovementioned topology, a two-channel air-filled SIW crossover is designed, as

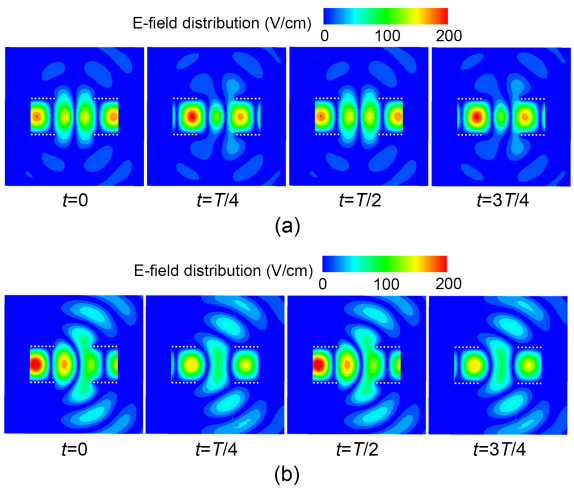

Fig. 3 E-field distribution with (a) and without (b) HCL at 30 GHz (*T* is the period of the electromagnetic field)

shown in Fig. 4a, where a_1 is the radius of the HCL of the two-channel crossover, d_1 is the distance between the centers of two adjacent metal holes, and d_2 is the diameter of the metal holes. The first step of the design procedure is to determine the relative dielectric constants inside and outside the HCL. To simplify the fabrication, an air-filled area is built by drilling the substrate. In this way, one can obtain an interface between two materials within a single substrate. Here, a Rogers RT/duroid 5880 substrate with a thickness of 0.787 mm is applied. Then, we have ε_{r1}=1.0 and ε_{r2}=2.2. Secondly, the width of the open air-filled SIW w should be large enough to support the dominant mode within the interested frequency spectrum. In this work, w=7.2 mm is chosen. Then, one open air-filled SIW should be duplicated to four and placed clockwise to build a closed cavity. Finally, an HCL is inserted at the center and its diameter is optimized to achieve the minimum reflection and isolation.

The E-field distribution of the designed two-channel crossover at 30 GHz is displayed in Fig. 4b, in which a crossed transmission is observed. The simulated S-parameters of the designed two-channel crossover are plotted in Fig. 4c, where S_{11} is the reflection coefficient of port 1, S_{21} is the isolation coefficient of port 1 and port 2, and S_{31} is the isolation coefficient of port 1 and port 3. From 25.8 to 38.3 GHz, the reflection coefficient and the isolation coefficients are lower than −15 dB, indicating a fractional bandwidth (FBW) of 39%. Within this frequency range, the insertion loss varies from 0.1 to 0.5 dB.

To describe the design process more clearly, parametric study is given in Section 2 of the supplementary materials. In the above, the design details of the two-channel air-filled SIW crossover have been elaborated. Interestingly, the proposed method can be directly extended to crossovers with more channels. As shown in Fig. 5a, a three-channel air-filled SIW crossover is designed using the proposed topology. Since the design process and operation principle are similar to those in the two-channel case, only the final model and simulation results are provided here. The E-field distribution at 34 GHz is displayed in Fig. 5b, in which a cross-passing property is observed. The optimal S-parameters are plotted in Fig. 5c. Due to the symmetry of the configuration, S_{51} and S_{61} are omitted. From 31.9 to 36.6 GHz, both the reflection and isolation coefficients are less than −15 dB; i.e., the FBW is 14%. Within this frequency

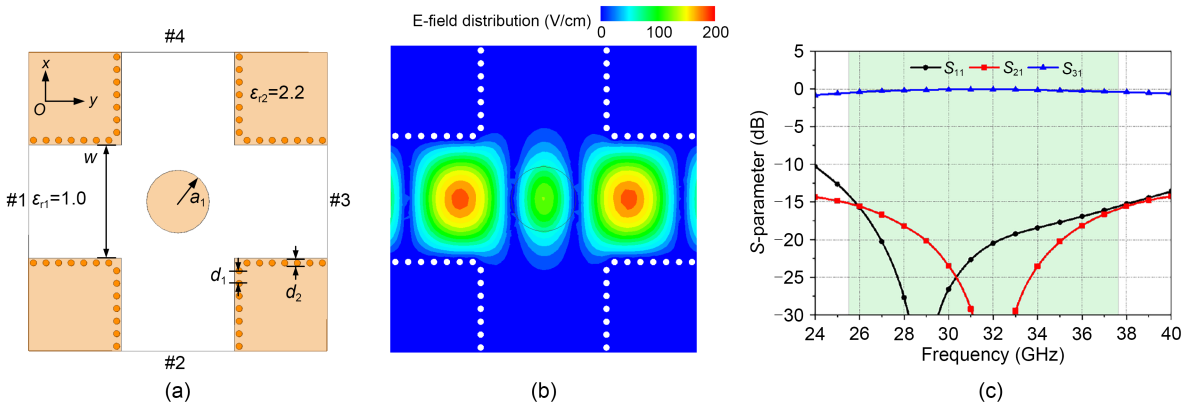

Fig. 4 Simulated HFSS model (a), E-field distribution (b), and *S*-parameters (c) of the two-channel SIW crossover (d_1= 0.80 mm, d_2=0.40 mm, a_1=2.00 mm, and w=7.20 mm)

Reprinted from Geng et al. (2022), Copyright 2022, with permission from IEEE

range, the minimum and maximum transmission losses are 0.1 dB and 0.7 dB, respectively.

Similarly, a four-channel counterpart is designed (Fig. 6a), and its E-field distribution is shown (Fig. 6b). Indicated by the *S*-parameters in Fig. 6c, the FBW is 7.5% (32.0 to 34.5 GHz). The minimum insertion loss is 0.2 dB, while the maximum insertion loss is 0.7 dB.

3 Results and discussion

3.1 Simulation and measurement

For the experiments, transitions from SIW to air-filled SIW and coplanar waveguide (CPW) to SIW are designed, as shown in Fig. 7a (Parment et al., 2015). The simulated reflection and transmission coefficients are plotted in Fig. 7b. From 25.9 to 41.6 GHz, the reflection coefficient is below −15 dB, corresponding to a maximum insertion loss of 0.8 dB and a minimum insertion loss of 0.4 dB. The fabricated prototypes of the two-, three-, and four-channel air-filled SIW crossovers are shown in Fig. 8. The interior, top, and bottom views are illustrated in Figs. 8a–8c. Two aluminum plates are added on the top and bottom of the substrate to act as ground planes. The design parameters of the crossover are listed in Table 1.

To describe the experimental results more clearly, an analysis based on the simulated and measured results of the crossovers is given in Section 3 of the supplementary materials for a detailed description. It can be concluded that the largest difference between the simulation and the measurement is in the insertion loss, about 1.7 dB. This discrepancy comes mainly from the insertion loss of the connectors, that of the connection between the connectors and the CPW, and the fabrication tolerance. The additional insertion loss mentioned

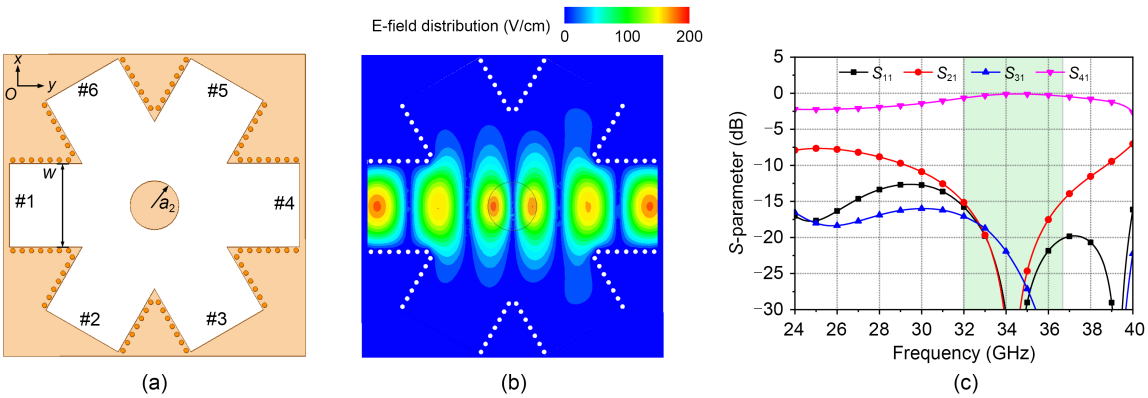

Fig. 5 Simulated HFSS model (a), E-field distribution (b), and *S*-parameters (c) of the three-channel SIW crossover (a_2= 2.10 mm, w=7.20 mm)

a_2 is the radius of the HCL of the three-channel SIW crossover, and S_{41} is the isolation coefficient of port 1 and port 4

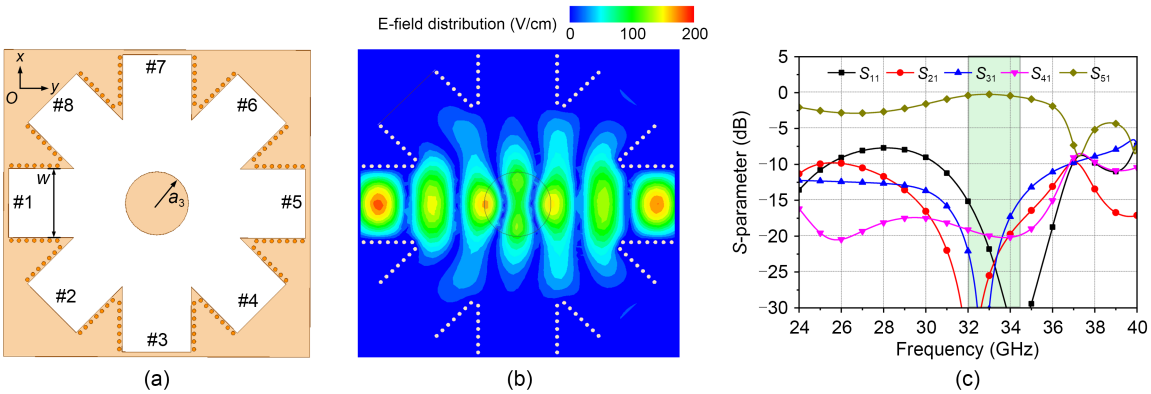

Fig. 6 Simulated HFSS model (a), E-field distribution (b), and *S*-parameters (c) of the four-channel SIW crossover (a_3= 4.00 mm, w=7.20 mm)

a_3 is the radius of the HCL of the four-channel SIW crossover, and S_{51} is the isolation coefficient of port 1 and port 5

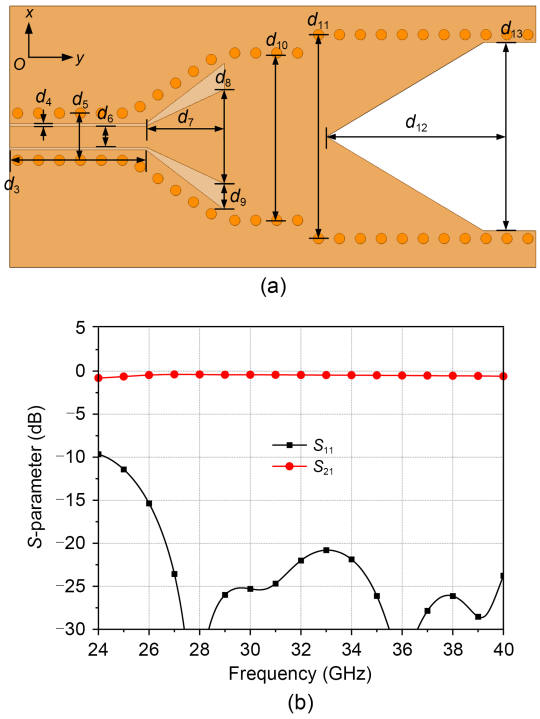

Fig. 7 Simulated HFSS model (a) and *S*-parameters (b) of the transition

d_3–d_{13} represent the sizes of the transition from SIW to air-filled SIW and coplanar waveguide to SIW within the HFSS model

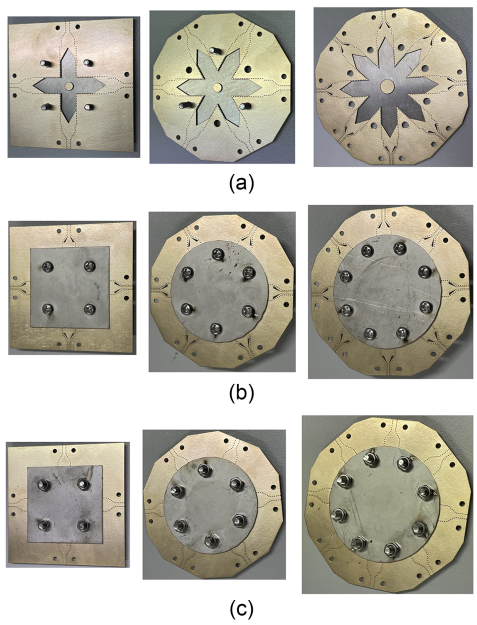

Fig. 8 Interior (a), top (b), and bottom (c) views of the fabricated prototypes (two-channel, three-channel, and four-channel crossovers from left to right)

above can be calibrated by using a thru-reflect-line (TRL) calibration to correct the effects of connectors and transitions, to correct characterize the demonstrator. The details of the calibration process are demonstrated in Doghri et al. (2015).

Table 1 Design parameters and values

Parameter	Value (mm)	Parameter	Value (mm)
d_1	0.80	d_{10}	6.40
d_2	0.40	d_{11}	7.80
d_3	5.20	d_{12}	6.90
d_4	0.10	d_{13}	7.20
d_5	1.80	a_1	2.00
d_6	0.80	a_2	2.10
d_7	3.00	a_3	4.00
d_8	3.60	w	7.20
d_9	1.00	h	0.787

3.2 Discussion

The comparisons between the proposed air-filled SIW crossovers and similar designs with two or more channels are summarized in Tables 2 and 3, respectively. It is concluded that using microstrip line can build extraordinarily compact two-channel crossover (Tajik et al., 2018). However, the microstrip line as an open structure would lead to increased loss operating at higher frequencies. Considering designs in the literature (Djerafi and Wu, 2009; Hesari and Bornemann, 2017; Ali and Sebak, 2018; Sun et al., 2020), it is noted that all of them suffer from relatively small bandwidth and large footprint when using either SIW or printed ridge gap waveguide technology. This brings the advantage of the proposed method in two-channel crossover designs; that is, the two-channel air-filled SIW crossover has a large FBW of 33% in the simulation and a reduced size of $0.74\lambda\times0.74\lambda$ (λ is the free-space wavelength at the center frequency). For fair comparisons, the FBW result is extracted from the complete model in the simulation including the SIW crossover and the transitions from air-filled SIW to CPW, and the size is related to the coupling area, which is surrounded by the open air-filled SIWs.

Table 3 describes crossovers with more than two channels. It can be seen that using a microstrip can build similar compact crossovers (Wu et al., 2014; Tang and Chuang, 2015; Chu and Tang, 2018). However, SIW technologies usually suffer from a larger footprint (Lian et al., 2020; Zhou and Wu, 2020). The designed three- and four-channel crossovers effectively reduce the occupied areas while maintaining sufficient FBWs.

Table 2 Comparisons between the designed two-channel crossovers and similar designs

Reference	Frequency (GHz)	Design technology	Simulated, measured bandwidth	Dimension ($\lambda\times\lambda$)	Insertion loss (dB)	Reflection loss (dB)	Isolation (dB)
Tajik et al., 2018	20.00	Microstrip line	DC-40, DC-35	0.20×0.20	0.35	21	19
Hesari and Bornemann, 2017	24.75	SIW	12.0%, 10.0%	About 1.70×1.70	1.10	17	23
Sun et al., 2020	10.20	SIW	6.5%, 6.0%	1.65×0.96	2.00	About 18	30
Djerafi and Wu, 2009	60.00	SIW	5.0%, 1.5%	NA	0.52	13	20
Ali and Sebak, 2018	30.00	Printed ridge gap waveguide	13.3%, 12.5%	1.50×1.50	0.50	10	15
This paper	31.00	SIW	33.0%, 30.0%	0.74×0.74	0.90	15	15

NA: not available

Table 3 Comparisons between the designed multi-channel crossovers and similar designs

Reference	Frequency (GHz)	Number of channels	Design technology	Simulated, measured bandwidth	Dimension ($\lambda\times\lambda$)	Insertion loss (dB)	Reflection loss (dB)	Isolation (dB)
Tang and Chuang, 2015	2.4	3	Microstrip line	13.5%, 13.7%	0.54×0.54	0.50	15	15
Chu and Tang, 2018	5.0	4	Microstrip line	2.6%, 1.5%	1.39×1.39	NA	15	16
Wu et al., 2014	1.0	3	Microstrip line	6.0%, 4.8%	0.31×0.29	1.00	15	15
Lian et al., 2020	10.0	4	SIW	10.0%, 10.0%	2.60×2.60	0.43	15	12
Zhou and Wu, 2020	13.0	5	SIW	NA, NA	3.50×1.90	0.90	10	13
This paper	34.4	3	SIW	14.0%, 6.5%	1.43×1.43	1.00	15	15
This paper	32.8	4	SIW	10.0%, 6.2%	1.90×1.90	1.10	15	15

NA: not available

4 Conclusions

In this work, a new method of crossover designs is presented by introducing an HCL in the middle of the air-filled SIW crossover cavity. According to ray-tracing analysis, the introduced HCL can concentrate and direct the electromagnetic wave in the desired direction and suppress the scattering within the cavity. Two-, three-, and four-channel air-filled SIW crossovers are designed and fabricated successively to demonstrate the feasibility of the proposed method. The corresponding FBWs of these cases in the simulation are 33%, 14%, and 10%, separately. The dimensions of their core areas are only $0.74\lambda\times0.74\lambda$, $1.43\lambda\times1.43\lambda$, and $1.90\lambda\times1.90\lambda$, separately. Compared with similar approaches, the designed crossovers show the merits of simple structure, compactness, and wide FBWs.

Contributors

Chun GENG and Jiwei LIAN designed the research. Chun GENG processed the data. Chun GENG and Jiwei LIAN drafted the paper. Dazhi DING revised and finalized the paper.

Compliance with ethics guidelines

Chun GENG, Jiwei LIAN, and Dazhi DING declare that they have no conflict of interest.

Data availability

The data that support the findings of this study are available from the corresponding author upon reasonable request.

References

Ali MMM, Sebak A, 2018. Compact printed ridge gap waveguide crossover for future 5G wireless communication system. *IEEE Microw Wirel Compon Lett*, 28(7):549-551. https://doi.org/10.1109/LMWC.2018.2835149

Bekefi G, Farnell GW, 1956. A homogeneous dielectric sphere

as a microwave lens. *Can J Phys*, 34(8):790-803. https://doi.org/10.1139/p56-089

Boriskin AV, Godi G, Sauleau R, et al., 2008. Small hemielliptic dielectric lens antenna analysis in 2-D: boundary integral equations versus geometrical and physical optics. *IEEE Trans Antenn Propag*, 56(2):485-492. https://doi.org/10.1109/TAP.2007.915432

Cheng XH, Liu ZY, Yao Y, et al., 2021. A wideband E-plane crossover coupler for terahertz applications. *China Commun*, 18(5):245-254. https://doi.org/10.23919/JCC.2021.05.015

Chu PC, Tang CW, 2018. Design of a compact planar crossover with four intersecting channels. *IEEE Microw Wirel Compon Lett*, 28(4):293-295. https://doi.org/10.1109/LMWC.2018.2811246

Costa JR, Lima EB, Fernandes CA, 2009. Compact beam-steerable lens antenna for 60-GHz wireless communications. *IEEE Trans Antenn Propag*, 57(10):2926-2933. https://doi.org/10.1109/TAP.2009.2029288

Djerafi T, Wu K, 2009. 60 GHz substrate integrated waveguide crossover structure. Proc European Microwave Conf, p.1014-1017. https://doi.org/10.23919/EUMC.2009.5296165

Doghri A, Djerafi T, Ghiotto A, et al., 2015. Substrate integrated waveguide directional couplers for compact three-dimensional integrated circuits. *IEEE Trans Microw Theory Tech*, 63(1):209-221. https://doi.org/10.1109/TMTT.2014.2376560

Feng WJ, Zhang TY, Che WQ, et al., 2016. Compact single-/dual-band planar crossovers based on strong coupled lines. *IEEE Trans Compon Packag Manuf Technol*, 6(6):854-863. https://doi.org/10.1109/TCPMT.2016.2555992

Geng C, Lian JW, Ding DZ, 2022. Wideband millimeter-wave SIW two-channel crossover based on homogeneous cylindrical lens. IEEE 10th Asia-Pacific Conf on Antennas and Propagation, p.1-2. https://doi.org/10.1109/APCAP56600.2022.10069830

Gunderson L, 1972. An electromagnetic analysis of a cylindrical homogeneous lens. *IEEE Trans Antenn Propag*, 20(4):476-479. https://doi.org/10.1109/TAP.1972.1140224

Hesari SS, Bornemann J, 2017. Substrate integrated waveguide crossover formed by orthogonal TE_{102} resonators. 47th European Microwave Conf, p.17-20. https://doi.org/10.23919/EuMC.2017.8230788

Jiao LX, Wu YL, Zhuang Z, et al., 2018. A wideband uniplanar double-ring crossover with balanced and single-ended paths. *IEEE Trans Microw Theory Tech*, 66(12):5238-5247. https://doi.org/10.1109/TMTT.2018.2865565

Li YJ, Luk KM, 2016. A multibeam end-fire magnetoelectric dipole antenna array for millimeter-wave applications. *IEEE Trans Antenn Propag*, 64(7):2894-2904. https://doi.org/10.1109/TAP.2016.2554601

Lian JW, Ban YL, Yang QL, et al., 2018. Planar millimeter-wave 2-D beam-scanning multibeam array antenna fed by compact SIW beam-forming network. *IEEE Trans Antenn Propag*, 66(3):1299-1310. https://doi.org/10.1109/TAP.2018.2797873

Lian JW, Ban YL, Zhu JQ, et al., 2019. Planar 2-D scanning SIW multibeam array with low sidelobe level for millimeter-wave applications. *IEEE Trans Antenn Propag*, 67(7):4570-4578. https://doi.org/10.1109/TAP.2019.2907377

Lian JW, Ban YL, Zhu H, et al., 2020. Uniplanar beam-forming network employing eight-port hybrid couplers and crossovers for 2-D multibeam array antennas. *IEEE Trans Microw Theory Tech*, 68(11):4706-4718. https://doi.org/10.1109/TMTT.2020.2992026

Lin JY, Wong SW, Wu YM, et al., 2019. Three-way multiple-mode cavity filtering crossover for narrowband and broadband applications. *IEEE Trans Microw Theory Tech*, 67(3):896-905. https://doi.org/10.1109/TMTT.2018.2886835

Niu ZQ, Zhang B, Li DT, et al., 2021. A mechanical reliability study of 3-dB waveguide hybrid couplers in submillimeter and terahertz bands. *Front Inform Technol Electron Eng*, 22(8):1104-1113. https://doi.org/10.1631/FITEE.2000229

Parment F, Ghiotto A, Vuong TP, et al., 2015. Air-filled substrate integrated waveguide for low-loss and high power-handling millimeter-wave substrate integrated circuits. *IEEE Trans Microw Theory Tech*, 63(4):1228-1238. https://doi.org/10.1109/TMTT.2015.2408593

Qi ZH, Li XP, Zhu H, 2021. Low-cost high-order-mode cavity backed slot array antenna using empty substrate integrated waveguide for the 5G n260 band. *Front Inform Technol Electron Eng*, 22(4):609-614. https://doi.org/10.1631/FITEE.2000503

Schoenlinner B, Wu XD, Ebling JP, et al., 2002. Wide-scan spherical-lens antennas for automotive radars. *IEEE Trans Microw Theory Tech*, 50(9):2166-2175. https://doi.org/10.1109/TMTT.2002.802331

Sun L, Deng HW, Xue YF, et al., 2020. Compact-balanced BPF and filtering crossover with intrinsic common-mode suppression using single-layered SIW cavity. *IEEE Microw Wirel Compon Lett*, 30(2):144-147. https://doi.org/10.1109/LMWC.2020.2965530

Tajik A, Fakharzadeh M, Mehrany K, 2018. DC to 40-GHz compact single-layer crossover. *IEEE Microw Wirel Compon Lett*, 28(8):642-644. https://doi.org/10.1109/LMWC.2018.2843134

Tang CW, Chuang WM, 2015. Design of the planar six-port crossover with double rings. *IEEE Microw Wirel Compon Lett*, 25(10):651-653. https://doi.org/10.1109/LMWC.2015.2463225

Wu LS, Mao JF, 2016. A planar filtering crossover for three intersecting channels. IEEE MTT-S Int Microwave Symp, p.1-3. https://doi.org/10.1109/MWSYM.2016.7540281

Wu LS, Guo YX, Mao JF, 2014. A planar microstrip crossover with lumped inductors for three intersecting channels. *IEEE Trans Microw Theory Tech*, 62(4):851-860. https://doi.org/10.1109/TMTT.2014.2309558

Xu HX, Wang GM, Chen PL, et al., 2011. Miniaturized fractal-shaped branch-line coupler for dual-band applications based on composite right/left handed transmission lines. *J Zhejiang Univ-Sci C (Comput & Electron)*, 12(9):766-773. https://doi.org/10.1631/jzus.C1000343

Yao JJ, Lee C, Yeo SP, 2011. Microstrip branch-line couplers for crossover application. *IEEE Trans Microw Theory Tech*, 59(1):87-92. https://doi.org/10.1109/TMTT.2010.2090695

Yu X, Sun S, 2019. Design of wideband lumped crossovers with resonator-loaded window shape structure. *IEEE Microw Wirel Compon Lett*, 29(5):309-311.

https://doi.org/10.1109/LMWC.2019.2907166

Zhan WL, Xu JX, Zhao XL, et al., 2020. Substrate integrated waveguide multi-channel filtering crossover with extended channel number and controllable frequencies. *IEEE Trans Circ Syst II Exp Briefs*, 67(12):2858-2862. https://doi.org/10.1109/TCSII.2020.2982409

Zhang J, Wu W, Fang DG, 2011. 360° scanning multi-beam antenna based on homogeneous ellipsoidal lens fed by circular array. *Electron Lett*, 47(5):298-300. https://doi.org/10.1049/el.2010.3646

Zhou K, Wu K, 2020. Multi-channel SIW filtering crossover with flexibly specified frequencies and bandwidths. IEEE USNC-CNC-URSI North American Radio Science Meeting (Joint with AP-S Symp), p.117-118. https://doi.org/10.23919/USNC/URSI49741.2020.9321671

List of supplementary materials

1 Supplement to the operation principle
2 Supplement to the design process
3 Supplement to the experiment